Controlling Electrospun Nanofiber Morphology and Mechanical Properties Using Humidity

Liwei Huang, Nhu-Ngoc Bui, Seetha S. Manickam, Jeffrey R. McCutcheon

Department of Chemical, Materials & Biomolecular Engineering, Center for Environmental Sciences and Engineering, University of Connecticut, Storrs, Connecticut 06269-3222

Correspondence to: J. R. McCutcheon (E-mail: jeff@engr.uconn.edu)

Received 3 May 2011; revised 9 August 2011; accepted 10 August 2011; published online 17 October 2011
DOI: 10.1002/polb.22371

ABSTRACT: Electrospinning is a fiber spinning technique used to produce nanoscale polymeric fibers with superior interconnectivity and specific surface area. The fiber diameter, surface morphology, and mechanical strength are important properties of electrospun fibers that can be tuned for diverse applications. In this study, the authors investigate how the humidity during electrospinning influences these specific properties of the fiber mat. Using two previously uninvestigated polymers, poly(acrylonitrile) (PAN) and polysulfone (PSU) dissolved in *N,N*-Dimethylformamide (DMF), experimental results show that increasing humidity during spinning causes an increase in fiber diameter and a decrease in mechanical strength. Moreover, surface features such as roughness or pores become evident when electrospinning in an atmosphere with high relative humidity (RH). However, PAN and PSU fibers are affected differently. PAN has a narrower distribution of fiber diameter regardless of the RH, whereas PSU has a wider and more bimodal distribution under high RH. In addition, PSU fibers spun at high humidity exhibit surface pores and higher specific surface area whereas PAN fibers exhibit an increased surface roughness but no visible pores. These fiber morphologies are caused by a complex interaction between the nonsolvent (water), the hygroscopic solvent (DMF), and the polymer. © 2011 Wiley Periodicals, Inc. J Polym Sci Part B: Polym Phys 49: 1734–1744, 2011

KEYWORDS: electrospinning; mechanical strength; nonwoven; porous nanofibers; relative humidity

INTRODUCTION Electrospinning has been broadly exploited for fabricating nanosized polymeric fibers into nonwovens with high porosity and superior pore interconnectivity. Recent research efforts have focused on using this technique to fabricate both synthetic and natural polymeric nanofibers[1–4] for various applications including membrane filtration, tissue engineering, and electrode applications.[5–7] A fundamental understanding of how to control the electrospinning process and thus the formation, shape, morphology, and strength of electrospun fibers is essential for developing a better understanding of the process. Better control of the process will allow for the design of specific electrospinning conditions and materials for these various applications.

Electrospinning involves using polymer solution, which is extruded through a needle or dye that is supplied with a high voltage. The resulting charge accumulates on the needle or dye tip, generating an electromotive force that overcomes the surface tension of the solution. A polymer jet is ejected from the tip of the Taylor cone at great speed, and subsequent whipping of the fiber results exceedingly high drawdown ratios. During the traveling of the jet toward a grounded collector, the solvent evaporates and causes the polymer to solidify into a fiber. These fibers are deposited randomly to form a nonwoven matrix onto the collector surface.

It is well known that the electrospinning process and the resulting properties of electrospun nanofibers can be manipulated by a number of variables. These parameters can be classified as solution properties, process conditions and ambient parameters. It was found that solution properties can affect the surface morphology of electrospun fibers. Generally speaking, for a variety of polymers, increasing concentration in solution yields larger fiber diameters and reduces the formation of beads.[8] However, Deitzel et al. observed a bimodal distribution of fibers for poly(ethylene oxide) solutions spun at high concentrations, which attributed to fiber-spraying events.[9] Studies have also investigated the effects of process parameters, such as flow rate and electric field strength, on fiber morphology and size. In general, it was found that lower flow rate, or higher voltage yielded fibers with smaller diameters.[10,11] However, if the voltage is too high, beads may form.[9]

Few studies have been conducted to examine the effects of ambient parameters (i.e., humidity) on the electrospinning process. Previous investigations have indicated that humidity can directly affect the fiber diameter. The diameter of

© 2011 Wiley Periodicals, Inc.

electrospun fibers from cellulose acetate were found to increase with increasing humidity while for poly(vinylpyrrolidone) the average diameter decreases.[12] There have also been investigations on humidity induced nanopore structure on fiber surface. Electrospun fibers from polystyrene (PS), polycarbonate, and poly(methyl methacrylate) were found to exhibit nanopores on the fiber surface in the presence of humidity when using highly volatile solvents. These submicron surface features were not observed in the absence of humidity.[13] It was also found that increasing humidity causes an increase in the number and size of nanopores.[14] The nanopore structure can be further controlled by adjusting other spinning conditions as well as the polymer/solvent properties. For instance, the nanoporosity of poly(oxymethylene) (POM) e-pun fibers could be decreased by increasing the oxyethylene unit in the POM copolymer, increasing the spinning voltage, as well as decreasing the solvent vapor pressure.[15] Lin et al. also studied the effect of solvent ratio on the nanoporous morphology of PS fibers. They found that by increasing the *N*,*N*-Dimethylformamide (DMF) ratio in the tetrahydrofuran/DMF solvent mixtures, the nanopores disappeared, replaced by wrinkled or smooth fiber surfaces.[16]

Even though these studies were successful in achieving porous nanofibers with specific polymers, the mechanism behind the formation of porous fibers during electrospinning is not sufficiently understood. Phase separation and evaporative cooling theory are two most popular mechanisms that have been used to explain this phenomenon. Phase separation theory suggests that, during solvent evaporation, the solution cools and undergoes thermal phase separation.[13,14,17,18] As evaporation occurs, the surface cools and results in thermally induced phase separation, which forms a skin layer on the spinning fiber. This effect is exacerbated by presence of water (a nonsolvent) in the air near the jet. This formation of the skin layer effectively locks the fiber into a larger diameter while dissolved polymer solution remains trapped in the core. Eventually, the solvent molecules in the core evaporate through the skin layer, leaving pores on the fiber surface.

The other mechanism to be considered in the formation of these surface nanopores is evaporative cooling, also called the "breath figures" mechanism, which was recently described by Srinivasarao.[19] Evaporative cooling occurs as a result of rapid solvent evaporation, thus significantly cooling the surface of the jet during its travel from needle to collector. As the surface cools, water vapor molecules condense on the surface and grow in the form of droplets, which act as hard spheres. As the jet dries, the water droplets leave imprints on the surface which are observed as pores.

This work aims to investigate the influence of relative humidity (RH) on electrospinning of two previously uninvestigated polymers: poly(acrylonitrile) (PAN) and polysulfone (PSU) dissolved in DMF. PAN is a hydrophilic polymer and has been widely used in filtration applications, such as ultrafiltration[20] and nanofiltration.[21] PAN nanofiber mats can also serve as a precursor to fabricate carbon nanofibers.[7,22,23] PSU, on the other hand, is a hydrophobic polymer that is commonly used in ultrafiltration[24] and reverse osmosis thin film composite membranes.[25] Both PAN and PSU nanofibers have recently been considered for filtration applications.[26–28]

If electrospun nanofibers are to be considered for a growing number of uses, we must be able to tailor the properties of the nonwoven material to suit the intended application. For instance, small diameters and surface roughness or porosity may be deemed better for filtration or tissue engineering applications since they result in higher specific surface areas. Better mechanical properties, such as increased tensile strength, is preferred for filtration applications that may require hydraulic pressure.

To tune these properties, however, we must comprehensively understand how the electrospinning procedure impacts the resulting nanofiber mat. Recent studies using these two polymers have focused on controlling the solution and processing parameters to make better electrospun fibers.[29–32] In this study, we systematically investigate how RH of the spinning environment impacts the nanofiber mat properties. Understanding how RH impacts the nanofibers properties will ultimately allow for better control over the electrospinning process and tuning of nanofiber mat properties.

EXPERIMENTAL

Materials

PAN ($M_w = 150{,}000$) was purchased from Scientific Polymer Products (Ontario, NY). PSU (UDEL 3500, $M_w = 80{,}000$–86,000) was obtained from Solvay Advanced Polymers (Alpharetta, GA). DMF was acquired from Acros Organics (Geel, Belgium). Both polymers dissolved in DMF at 60 °C and the resulting homogeneous solutions were continuously stirred for 24 h.

Electrospinning

The PAN and PSU solutions were electrospun in a closed chamber to allow for humidity control. Venting is provided to prevent the DMF vapor from accumulating in the chamber. However, only small amounts of solution were spun (on the order of milliliters), thus preventing significant DMF vapor accumulation. A schematic of the custom built electrospinning apparatus is shown in Figure 1 (the venting and humidity control system are not shown). A polymer solution was placed in a 10-mL syringe attached to a syringe pump (Fisher Scientific, Pittsburgh, PA). A grounded stainless steel rotating drum, which served as a collector, was positioned at 18 cm from the needle tip, and a potential was applied using a high voltage power supply (Gamma High Voltage, Ormond Beach, FL). The RH was controlled by a humidity control system (ETS Microcontroller, Model 5100, Glenside, PA) utilizing a drierite column and a humidifier. House compressed air was supplied directly to the chamber for low humidity tests. The RH was held constant for each experiment, with an error range of ±2%. 0% RH condition was achieved by using dry compressed air and was additionally monitored using a NIST-certified hygrometer.

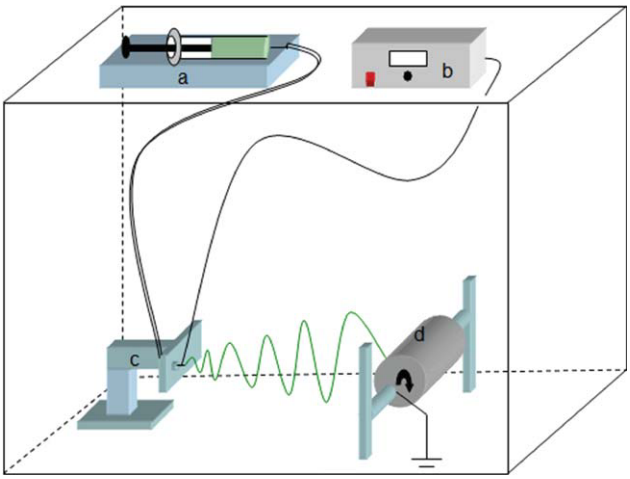

FIGURE 1 Schematic of electrospinning setup: (a) syringe pump with syringe, (b) high voltage supply, (c) transition stage, and (d) rotating grounded collector. The transition stage oscillates parallel to the collector drum, resulting in a nonwoven mat of uniform thickness.

For our experiments the RH was varied from 0 to 60% for electrospinning PAN and 0–50% for PSU. PAN and PSU fibers could not be spun at RH greater than 60 and 50%, respectively. Based on preliminary work not described here, we found that 10 wt % of PAN and 26 wt % of PSU (both in DMF) produced the most uniform fibers with relatively good mechanical strength compared to other concentrations. Using an applied voltage of 28 kV and with a flow rate of 1.0 mL/h, high-quality fibers with relatively few defects and beads could be spun throughout the whole humidity range. The spinning was conducted at room temperature, which varies between 21 and 22 °C. The chosen spinning parameters for this study are listed in Table 1.

Characterization

FEI Phenom scanning electron microscopy (SEM) from FEI Company (Hillsboro, OR) and field emission scanning electron microscopy (FESEM, JEOL 6335F) were used to observe the surface morphology (i.e., roughness and/or nanopore structure) and to estimate the diameter of the nanofibers. The samples were sputter-coated with gold or platinum before obtaining SEM or FESEM images. ImageJ software was used to determine the average fiber diameter and fiber size distribution using twenty fiber diameter measurements. The specific surface areas of electrospun samples were determined using a nitrogen adsorption surface analyzer (ASAP 2020, Micromeritics). Stress-strain curves for the electrospun fiber mats were obtained using A Tytron 250 Microforce Testing System (MTS Systems), from which the tensile strength and Young's modulus were derived. For characterization of mechanical properties, a minimum of three strips (40 mm × 6.5 mm) were cut from each sample.

RESULTS AND DISCUSSION

Effects of Humidity on Fiber Diameter

Figure 2 shows the SEM images and fiber size distribution of electrospun PAN nanofibers as a function of RH (0, 20, 40, and 60%) that correspond to the average fiber sizes given in Table 2. Similarly, Figure 3 shows the SEM images and fiber size distribution of electrospun PSU nanofibers at different RH (0, 20, 40, and 50%) with corresponding values of average fiber size given in Table 3.

As shown in these figures and tables, spinning at higher RHs led to larger PAN and PSU fibers. For instance, the average fiber diameter of PAN increased from 150 nm at 0% RH to 630 nm at 60% RH (Table 2), and the average fiber diameter of PSU increased from 1.15 μm at 0% RH to 3.58 μm at 50% RH (Table 3). These findings were in accordance with other published work showing that increasing humidity during spinning generally resulted in increased fiber diameter for other polymers.[14,17]

This phenomenon can occur for multiple reasons. Higher water vapor pressures result in more water molecules between the needle and collector. The presence of these water molecules decreases the amount of excess charges on the electrospinning jet due to molecular polarization.[17,27] As a consequence, the intensity of the electric field is decreased. Under a weaker field, the jets would experience a smaller drawdown force and thus undergo reduced elongation. These results agree with previous work that showed that as the applied voltage increases, both the jet diameter and fiber diameter decreases for PS[11,13] and POM polymers.[15] Furthermore, the presence of water vapor, which acts as a nonsolvent to both of these polymers, facilitates precipitation of the fiber before deposition of the collector surface. This accelerated precipitation locks in the fiber diameter before the rest of the solvent has a chance to evaporate.

Humidity was also shown to have some different effects on the fiber spinning of these two polymers. As seen in the diameter distribution plots (Fig. 2), PAN fiber diameters were reasonably uniform at all RHs (standard deviations from about 15–25%). For PSU, higher humidity resulted in a broad, almost bimodal distribution of fiber diameter. Distribution plots in Figure 3 indicate that at lower RHs (0 and 20%), the PSU nanofibers were relatively uniform and the fiber size followed a Gaussian-like distribution. At higher RHs (40 and 50%), the fiber size distributions became

TABLE 1 Experimental Conditions for Electrospinning PAN and PSU

Polymer	Solvent	Concentration (wt %)	Voltage (kV)	Flow rate (mL/h)	Rotating rate (rpm)	RH (%)	Temperature (°C)
PAN	DMF	10	28	1	70	0∼60	21–22
PSU	DMF	26	28	1	70	0∼50	21–22

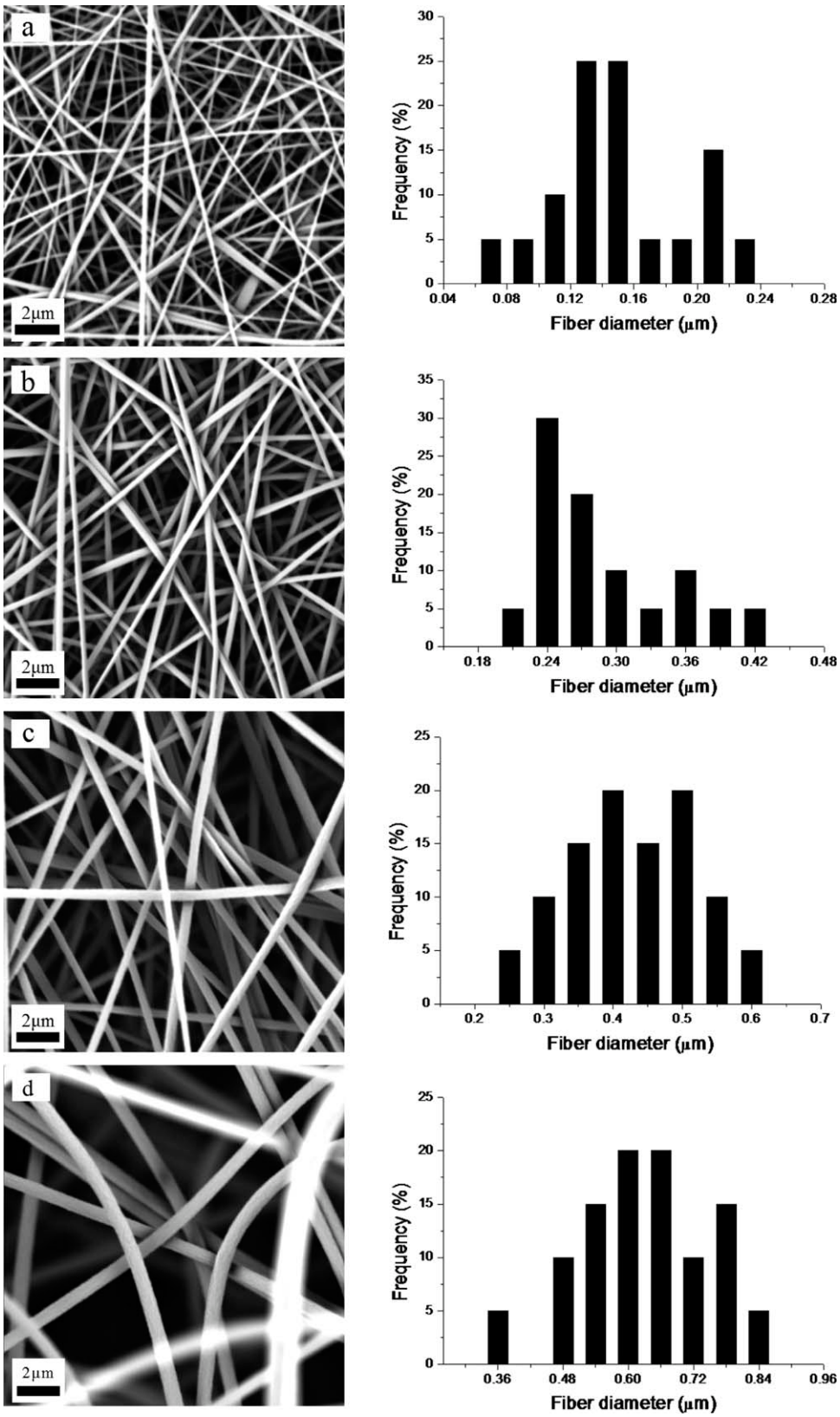

FIGURE 2 SEM images (magnification 15,000×) and fiber diameter distribution of PAN nanofibers spun at different RH: (a) 0% RH; (b) 20% RH; (c) 40% RH; and (d) 60% RH.

TABLE 2 Average PAN Fiber Diameter at Different RH

RH (%)	Average Diameter (μm)	Standard Deviation (μm)	Standard Deviation (%)
0	0.15	0.04	27
10	0.21	0.05	24
20	0.28	0.06	21
30	0.33	0.05	15
40	0.43	0.08	19
50	0.53	0.14	26
60	0.63	0.14	22

broader. The corresponding SEM images in Figure 3 illustrate that at higher RHs both large and small fibers are present. In addition, some beads were also observed amongst the PSU fiber at higher RHs. Table 3 indicates broadening of the fiber size distribution for PSU. At 50% RH, the standard deviation of the fiber size distribution is 84% of the mean.

A wider and more bimodal distribution is likely caused by the instability of the electrospinning process. It was found that during electrospinning at high humidity, the PSU fiber jet was unstable, thus creating broken fibers that may vary in fiber diameter along their length. This instability was not observed when spinning PAN at higher humidity.

There are several causes of this instability during the spinning of PSU. The 26% PSU is more viscous than the 10% PAN, thus making the PSU solution more sensitive to a decrease in the electric field strength at high humidity. The reduced drawdown force is less able to overcome the viscous forces of the high concentration PSU solution. This effect is less noticeable in the lower viscosity PAN solution. Furthermore, these polymers have a different tolerance to water in their solution form. In the presence of water molecules, both polymers experience vapor-induced phase separation, which causes thermodynamic instability. However, PSU will undergo phase separation more rapidly than PAN since it has a lower tolerance to water. The phase diagram for the PAN-DMF-H_2O ternary system[33] indicates that the water concentration in a 10% PAN solution can be about 10% (by mass) before it precipitates. PSU, on the other hand, cannot dissolve in DMF with even small amounts of water present.[34] As a consequence, the PSU rapidly demixes in the presence of water vapor, precipitating during spinning which destabilizes the jet and breaks fibers. The non-continuous jet forms broken fibers with slender and long tails before deposition, resulting in wide fiber size distributions for PSU fibers spun at higher RHs.

Effects of Humidity on Fiber Surface Morphology

Figures 4 and 5 show SEM images of PAN and PSU electrospun fibers with humidity induced surface morphology. Analysis of Figures 4 and 5 indicates that humidity significantly affected the fiber surface structure. For instance, for PAN, at very low RH (0%), the fiber surface was very smooth. At higher RH, the fibers exhibited increased surface roughness. PSU, on the other hand, had a more complicated surface morphology transition with increasing RH. At very low RH (0%), the fiber surface exhibited elongated pores or creases. When humidity was increased to 10%, additional roughness appeared. At RH of 30% and higher, nanopores could be observed on the fiber surface. Further increasing the humidity resulted in a more porous surface. Similar results were reported by Casper et al., which showed that PS fibers only exhibited nanoporosity when spun at RH above above 31%. The nanoporosity could be increased by spinning at higher humidity.[14]

Both phase separation and evaporative cooling mechanisms can be used to explain the difference in fiber surface morphology between these two polymers. There was no pore formation on PAN fibers even at RH as high as 60%, but the PSU fiber surface exhibited surface nanopores at 30% RH and higher. From a phase separation point of view, this difference is credited to the fiber size. For example, the PAN fiber diameters were less than one micron under the evaluated RH range. Though higher humidity yielded larger and rougher fibers, nanopores were never observed on the surface. The PSU fibers spun at 10–20% RH were around 2 μm in diameter and exhibited roughness but did not contain observable nanopores. Nanopores were observed, however, at above 30% RH when the fiber size increased to about 3 μm. Fiber size likely plays a key role in nanopore formation given that larger fibers contain more entrapped solvent within their core. This solvent eventually evaporates, causing the formation of pores on the fiber surface. Previous studies have reported micron-size electrospun fibers containing entrapped solvent within the fiber core using an optical microscope.[35] The smaller the fiber diameter, the less solvent entrapped within the fiber and thus less evaporation and pore formation.

If we consider the breath figures mechanism caused by evaporative cooling, the difference in surface features might be due to the difference in hydrophobicity/hydrophilicity of these two polymers. Since PSU is hydrophobic, the surface will be less wetted by water. As more water molecules condense on the fiber surface they gradually grow into water droplets, which are then big enough to leave nanosized indentations on the fiber surface. PAN, on the other hand, is hydrophilic, and thus readily adsorbs water molecules. Water sorption into the solution (or into a precipitated skin layer) occurs quickly after adsorption, and thus large droplets do not form and leave observable indentations.

Effects of Humidity on Surface Area of Elctrospun Fiber Mats

Both fiber size and fiber surface features (i.e., roughness and nanopores) impact the specific surface area of a nanofiber nonwoven. Generally, smaller fiber size, surface roughness, and surface pores result in higher surface area. As discussed earlier, increasing humidity causes an increase in fiber size and gives rise to the formation of surface features, which are two opposing factors affecting surface area.

Table 4 shows the specific surface area of PAN and PSU nanofibers spun at different RH. There is a decreasing trend

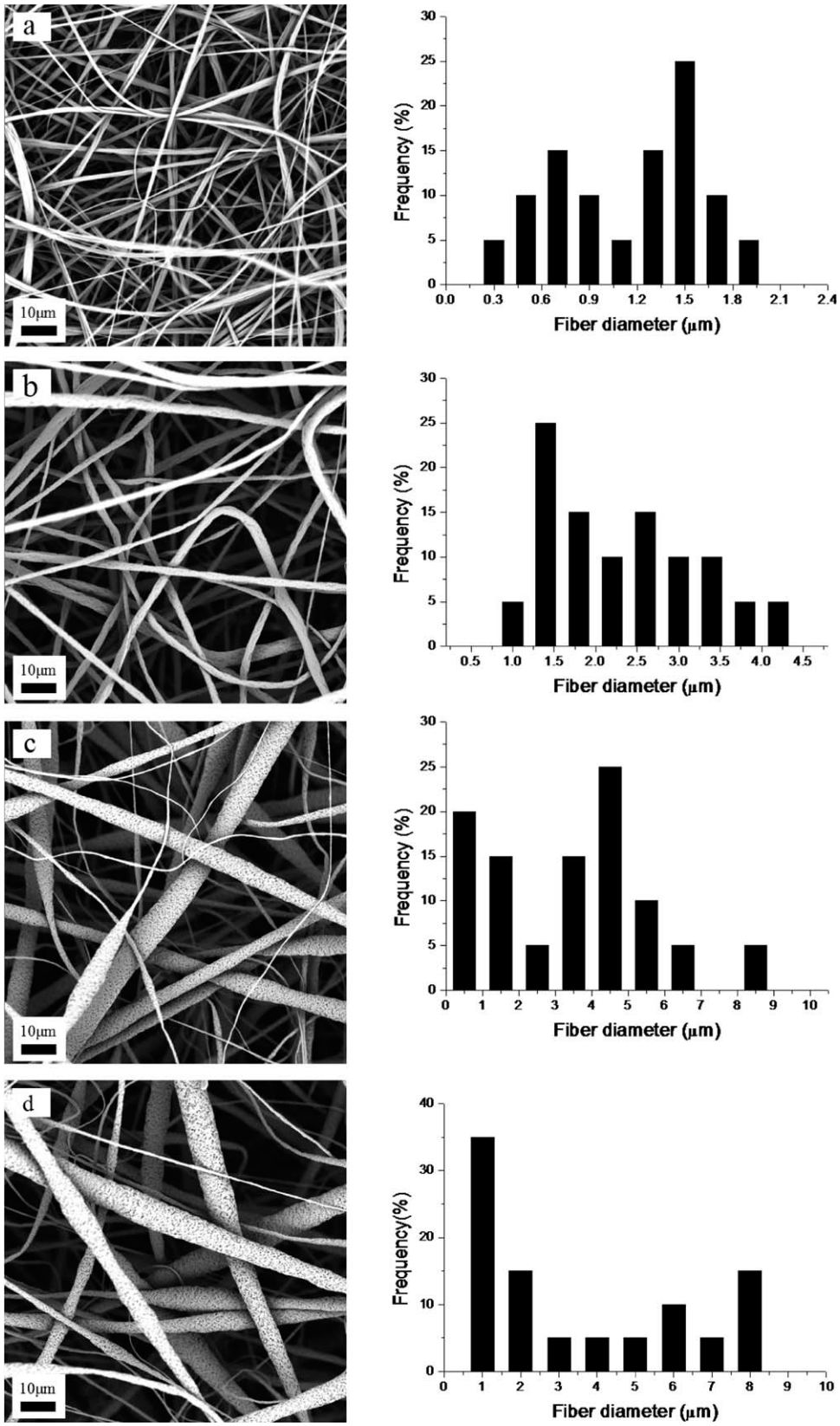

FIGURE 3 SEM images (magnification 2500×) and fiber diameter distribution of PSU nanofibers spun at different RH: (a) 0% RH; (b) 20% RH; (c) 40% RH; and (d) 50% RH.

TABLE 3 Average PSU Fiber Diameter at Different RH

RH (%)	Average Diameter (μm)	Standard Deviation (μm)	Standard Deviation (%)
0	1.15	0.46	40
10	1.61	0.40	25
20	2.29	0.90	39
30	3.19	1.57	49
40	3.26	2.08	64
50	3.58	3.00	84

of surface area for PAN from about 10 m^2/g at 0–20% RH to about 4 m^2/g at 60% RH, whereas for PSU, there is a dramatic increase from about 2.5 m^2/g at 0–20% RH to 21.7 m^2/g at 40% RH. The difference in surface area between the two polymers is caused by their different surface morphology. For PAN, increased fiber size at higher RH outweighs the increased fiber roughness, resulting in an overall decrease in specific surface area. For PSU, the surface area remains low or even decreases due to increased fiber size until nanopores form on the surface. When this occurs, of the presence of nanopores outweighs the effect of increased fiber size, thus resulting in an almost 10-fold increase in surface area.

These findings suggest that fiber nanoporosity can be induced in PSU nanofibers by simply adjusting RH during spinning. This method is simpler and arguably achieves better results than other reported methods. McCann et al. prepared nanoporous PAN fibers by electrospinning a solution into liquid nitrogen, followed by drying in vacuum. They found a three-fold increase in surface area compared to the smooth fibers.[36] Gupta prepared porous nylon-6 fibers by electrospinning a Lewis acid–base complex solution of nylon-6 and gallium trichloride ($GaCl_3$) followed by $GaCl_3$ removal. They reported a six-time increase in surface area upon formation of pores.[37] In comparison to these studies, the method shown here results in a larger increase in surface area, is broadly applicable to more polymers and is easily implemented into most existing electrospinning systems.

Effects of Humidity on Mechanical Properties of Elctrospun Fiber Mats

Electrospun nanofiber mats are highly porous but their mechanical strength is generally poor. Mechanical properties, often measured as tensile strength and Young's modulus, are dependent on both the strength of the individual fibers as well as bonding between fibers. The results below elucidate how the nonwoven's mechanical properties are affected by the RH during spinning.

Representative stress–strain curves of electrospun PAN fiber mats spun over a range of RH (0–40%) are shown in Figure 6. The average tensile strength and Young's modulus (both averaged from three separate samples) as a function of RH

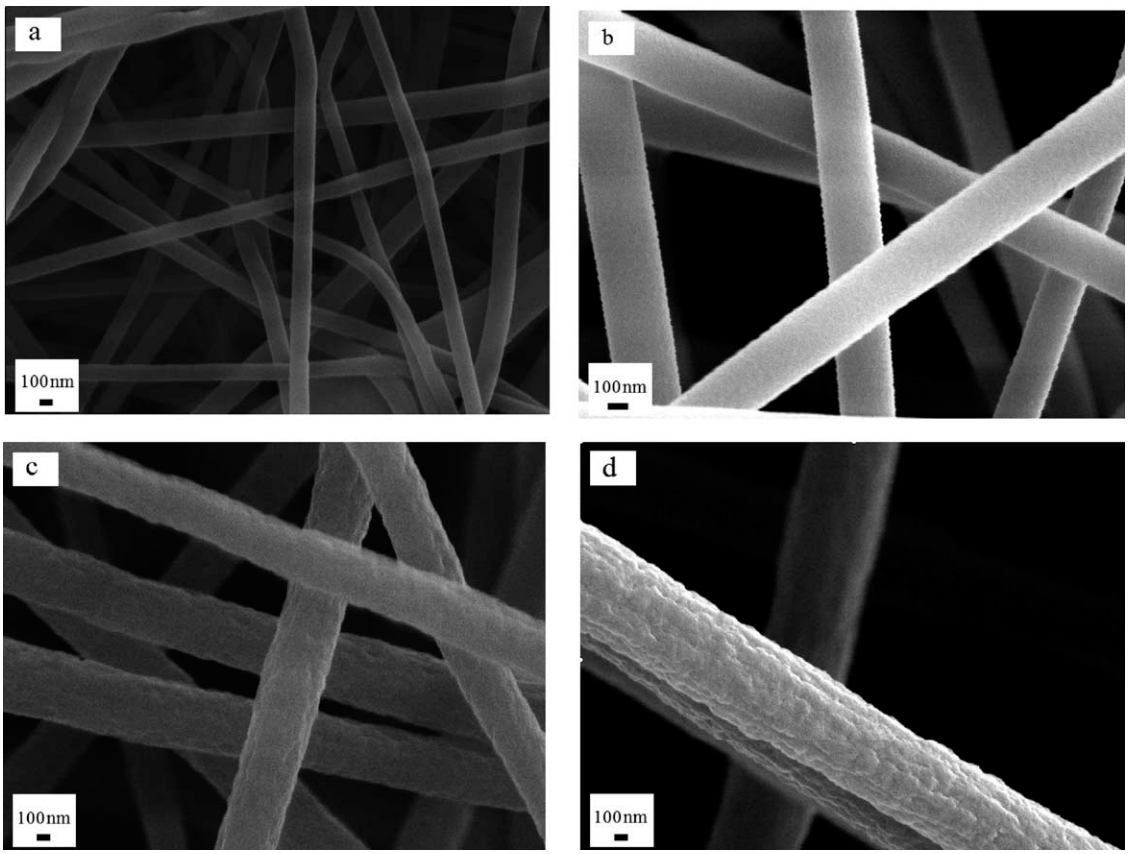

FIGURE 4 FESEM images of PAN nanofibers spun at different RH: (a) 0% RH; (b) 20% RH; (c) 40% RH; (d) 60% RH. The magnification of (a), (c) and (d) is 30,000× and of (b) is 45,000×.

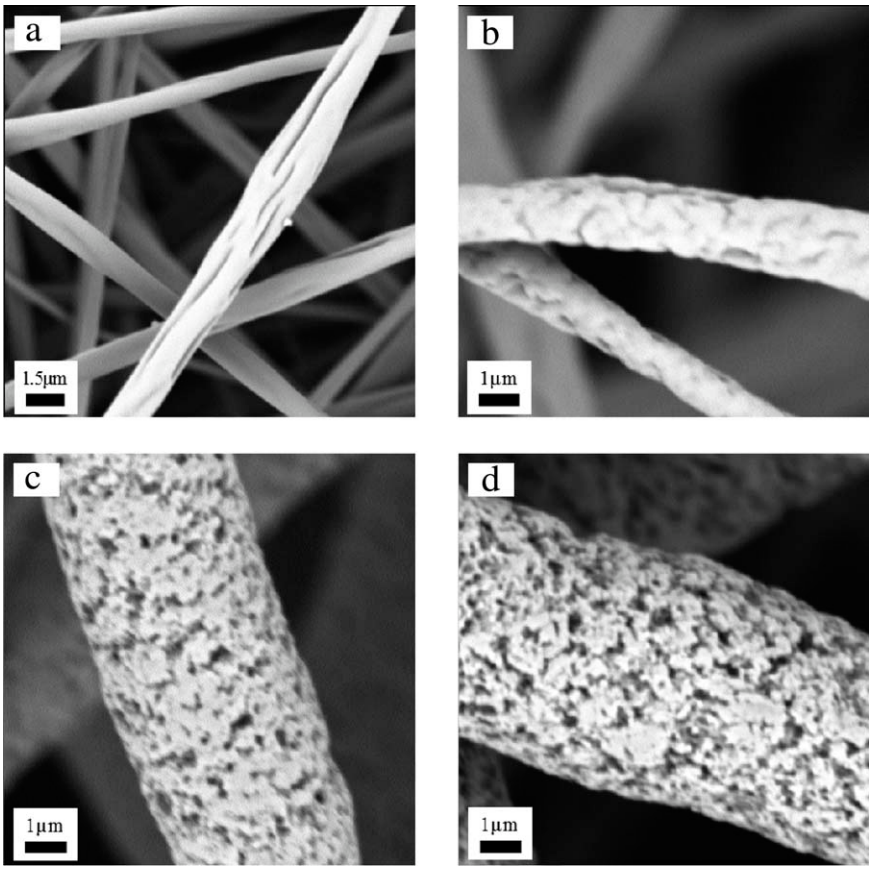

FIGURE 5 SEM images of PSU nanofibers spun at different RH: (a) 0% RH; (b) 10% RH; (c) 30% RH; (d) 50% RH. The magnification of (b), (c) and (d) is 24,000× and of (a) is 15,000×.

are shown in Figure 7(a,b), respectively. Results show that the PAN fiber mat was the strongest at 20% RH where it had the highest tensile strength (~6.25 MPa) and Young's modulus (~95 MPa). The mat exhibited the lowest tensile strength (~1.2 MPa and Young's modulus (~5 MPa) when spun at 40% RH. Both tensile strength and Young's modulus first increased with increasing RH then precipitously decreased.

Representative stress–strain curves of electrospun PSU fiber mats over a range of RH (0–40%) are shown in Figure 8. The average tensile strength and Young's modulus as a function of RH are shown in Figure 9(a,b), respectively. Results show that PSU fiber mat was strongest at 10% RH where it had the highest tensile strength (~1.65 MPa) and Young's modulus (~20 MPa). The mat exhibited the lowest tensile strength (~0.05 MPa) and Young's modulus (~1 MPa) when spun at 40% RH. Generally, these results mimicked those

TABLE 4 BET Surface Area of PAN and PSU at Different RH

Polymer	RH (%)	BET Surface Area (m^2/g)
PAN	0	8.00
	20	10.19
	60	4.21
PSU	0	2.72
	20	2.31
	40	21.74

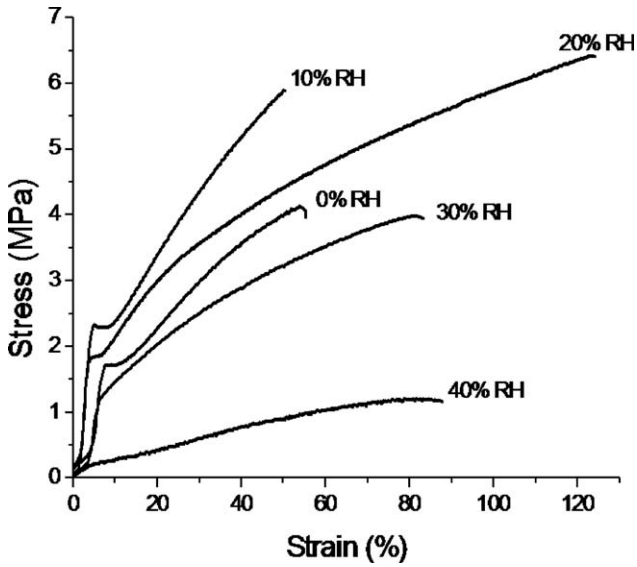

FIGURE 6 Representative stress–strain curves of PAN nanofibers spun at different RH.

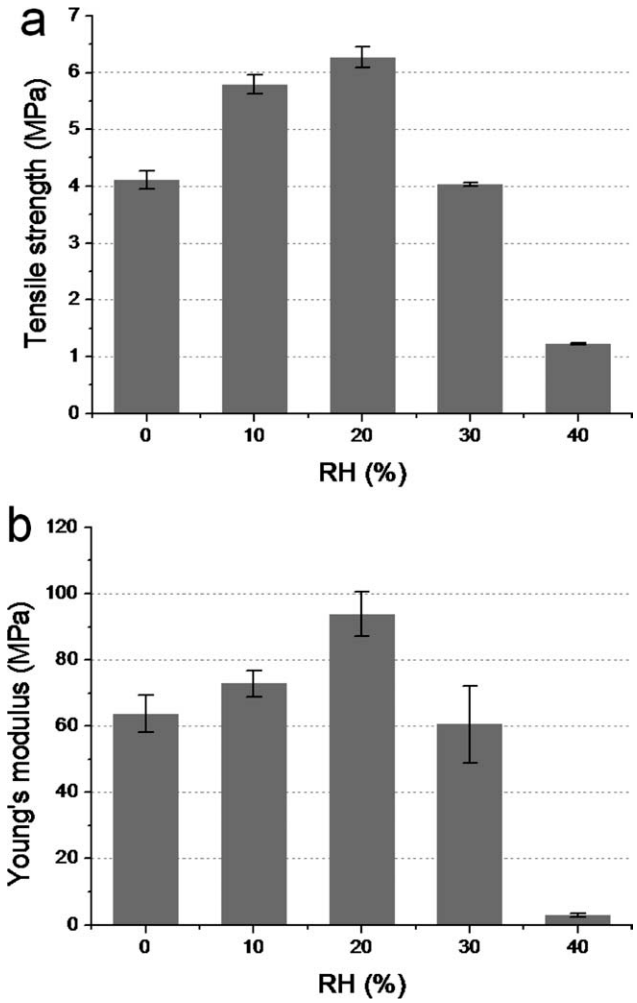

FIGURE 7 Mechanical properties of PAN nanofibers spun at different RH: (a) Tensile strength and (b) Young's modulus.

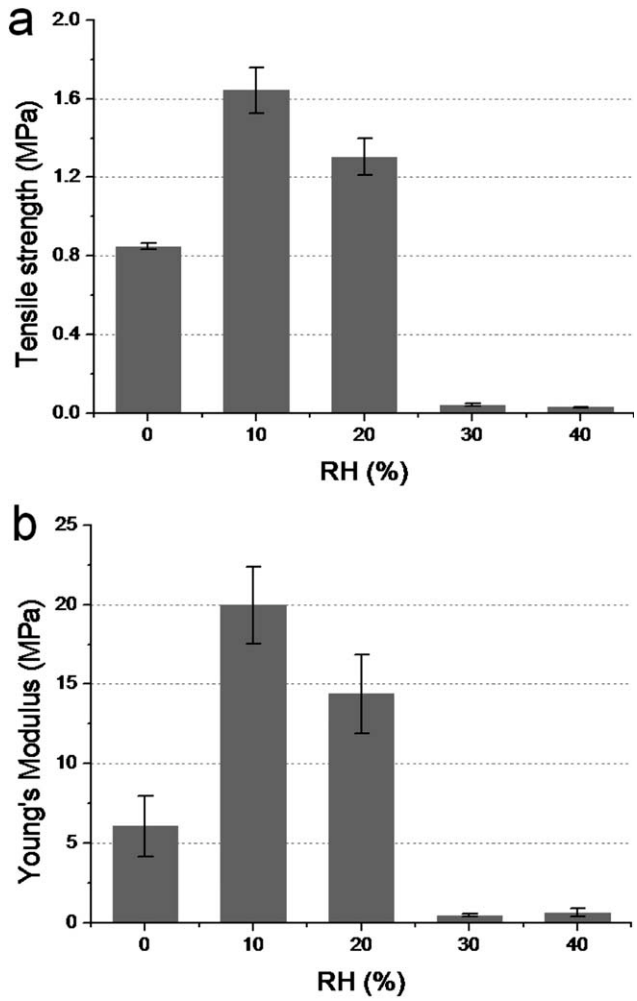

FIGURE 9 Mechanical properties of PSU nanofibers spun at different RH: (a) Tensile strength and (b) Young's modulus.

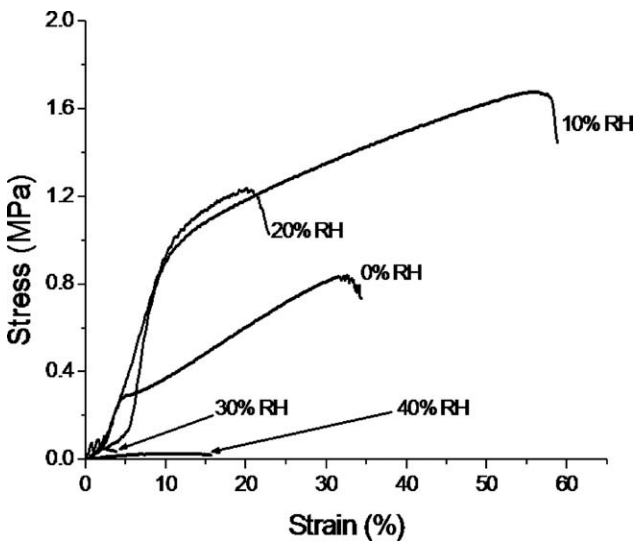

FIGURE 8 Representative stress–strain curves of PSU nanofibers spun at different RH.

obtained with the PAN fibers, though the mechanical strength of the PSU mats was noticeably lower when spun at the higher humidity.

Both results of PAN and PSU indicate that RH plays an important role in determining the mechanical properties of the nanofiber nonwoven. In general, electropsun fibers have better mechanical properties when spun at lower RH than those at high RH. This could be visually observed after the spinning was complete. At low RH, the fiber mat could be handled by hand and seemed uniform and well integrated. At high RH, the mats exhibited a fluffy, cotton-like texture indicating poor fiber–fiber bonding. The reason for this poor bonding at high RH is due to the phase separation promoted by the presence of water. A skin layer forms shortly after the polymer jet comes into contact with the surrounding environment. As the skin is formed, the amount of residual solvent on the skin surface is reduced. Therefore, fiber–fiber adhesion will be weaker as residual solvent is necessary to solder fiber junctions together.[27] This reduced strength is most acute in the PSU fiber mats spun at higher humidity.

As discussed earlier, PSU undergoes phase separation more quickly than PAN, thus resulting in faster skin formation. Furthermore, the nanoporous structure of the individual fibers also contributes to the lower strength due to a weaker individual fiber.

CONCLUSIONS

This investigation has demonstrated that the level of moisture in the air affects the diameter, surface morphology, and mechanical properties of electrospun PAN and PSU fibers. The fiber size of both PAN and PSU increased with increasing RH. However, the changes in fiber size distribution were quite different. PAN fibers were relatively uniform throughout the range of RHs examined. PSU, while maintaining uniformity at lower RH, formed both very large and very small fibers at higher RH and the resulting fiber size distributions were broad and bimodal. This difference results from the relative tolerances of these polymers to water. Dissolved PSU has less tolerance to water and thus experiences a faster phase separation. Higher RH during electrospinning also resulted in different surface morphologies of the PAN and PSU fibers. PAN fibers exhibited surface roughness when spun at high humidity while PSU fibers contained nanopores. The resulting morphology is dependent on the polymer chemistry (hydrophilicity), tolerance to water, and the fiber size. Nitrogen adsorption analysis indicated that both fiber size and nanopores affected specific surface area of the nonwoven mats spun from both polymers.

Humidity was also shown to impact the mechanical properties of both the PAN and PSU fiber mats. Generally, electrospun fibers at low RH had higher strength than those at high RH. Fibers spun at high RH underwent partial phase separation, resulting in a skin layer which hindered fiber–fiber bonding in the mat. This impacted PSU nanofibers to a greater extent due to PSU's rapid demixing in the presence of water vapor. The formation of nanopores on the fibers also has resulted in weakening of the PSU fibers.

These insights provided by this paper provide a stronger fundamental understanding of the electrospinning process over a range of humidity for a commercially available hydrophobic and hydrophilic polymer. This work indicates that humidity can be tuned to tailor fiber surface morphology and mechanical properties. These results are broadly applicable across many polymer materials and thus provide an additional independent variable for controlling fiber properties. This may enable electrospun fiber mats to be customized for a growing number of specific applications in filtration, nanocomposites, and tissue engineering.

ACKNOWLEDGMENTS

The authors graciously acknowledge the University of Connecticut Research Foundation, The University of Connecticut Center for Environmental Sciences and Engineering, the National Science Foundation (CBET-0933553), Oasys Water®, and the Department of Energy for financial support. The authors also thank Solvay Advanced Polymers for providing the polysulfone for this work.

REFERENCES AND NOTES

1 Reneker, D. H.; Chun, I. *Nanotechnology* **1996,** *7*, 216–223.

2 Doshi J.; Reneker, D. H. *J. Electrostat.* **1995,** *35*, 151–160.

3 Matthews, J. A.; Wnek, G. E.; Simpson, D. G.; Bowlin, G. L. *Biomacromolecules* **2002,** *3*, 232–238.

4 Xie, J. B.; Hsieh, Y. L. *J. Mater. Sci.* **2003,** *38*, 2125–2133.

5 Gopal R.; Kaur S.; Ma, Z. W.; Chan, C.; Ramakrishna, S.; Matsuura T. *J. Memb. Sci.* **2006,** *281*, 581–586.

6 Lannutti, J.; Reneker, D.; Ma, T.; Tomasko, D.; Farson, D. F. *Mater. Sci. Eng. C-Bio. Supramol. Syst.* **2007,** *27*, 504–509.

7 Kim, C.; Yang, K. S.; Lee, W. J. *Electrochem. Solid State Lett.* **2004,** *7*, A397–A399.

8 Pham, Q. P.; Sharma, U.; Mikos, A. G. *Tissue Eng.* **2006,** *12*, 1197–1211.

9 Deitzel, J. M.; Kleinmeyer, J.; Harris, D.; Tan, N. C. B. *Polymer* **2001,** *42*, 261–272.

10 Zong, X. H.; Kim, K.; Fang, D. F.; Ran, S. F.; Hsiao, B. S.; Chu B. *Polymer* **2002,** *43*, 4403–4412.

11 Wang, C.; Hsu, C. H.; Lin, J. H. *Macromolecules* **2006,** *39*, 7662–7672.

12 De Vrieze, S.; Van Camp, T.; Nelvig, A.; Hagstrom, B.; Westbroek, P.; De Clerck K. *J. Mater. Sci.* **2009,** *44*, 1357–1362.

13 Megelski, S.; Stephens, J. S.; Chase, D. B.; Rabolt, J. F. *Macromolecules* **2002,** *35*, 8456–8466.

14 Casper, C. L.; Stephens, J. S.; Tassi, N. G.; Chase, D. B.; Rabolt, J. F. *Macromolecules* **2004,** *37*, 573–578.

15 Kongkhlang, T.; Kotaki, M.; Kousaka, Y.; Umemura, T.; Nakaya, D.; Chirachanchai S. *Macromolecules* **2008,** *41*, 4746–4752.

16 Lin, J. Y.; Ding, B.; Yu, J. Y.; Hsieh Y. *ACS Appl. Mater. Interfaces* **2010,** *2*, 521–528.

17 Medeiros, E. S.; Mattoso, L. H. C.; Offeman, R. D.; Wood, D. F.; Orts, W. J. *Can. J. Chem.* **2008,** *86*, 590–599.

18 vandeWitte, P.; Dijkstra, P. J.; vandenBerg, J. W. A.; Feijen J. *J. Memb. Sci.* **1996,** *117*, 1–31.

19 Srinivasarao, M.; Collings, D.; Philips, A.; Patel S. *Science* **2001,** *292*, 79–83.

20 Musale, D. A.; Kumari, A.; Pleizier G. *J. Memb. Sci.* **1999,** *154*, 163–173.

21 Musale, D. A.; Kumar A. *J. Appl. Polym. Sci.* **2000,** *77*, 1782–1793.

22 Gu, S. Y.; Ren, J.; Wu, Q. L. *Synth. Met.* **2005,** *155*, 157–161.

23 Zussman, E.; Chen, X.; Ding, W.; Calabri, L.; Dikin, D. A.; Quintana, J. P.; Ruoff, R. S. *Carbon* **2005,** *43*, 2175–2185.

24 Nabe, A.; Staude, E.; Belfort G. *J. Memb. Sci.* **1997,** *133*, 57–72.

25 Song, Y. J.; Sun, P.; Henry, L. L.; Sun, B. H. *J. Memb. Sci.* **2005,** *251*, 67–79.

26 Yoon, K.; Kim, K.; Wang, X. F.; Fang, D. F.; Hsiao, B. S.; Chu B. *Polymer* **2006,** *47*, 2434–2441.

27 Tang, Z. H.; Qiu, C. Q.; McCutcheon, J. R.; Yoon, K.; Ma, H. Y.; Fang, D. F.; Lee, E.; Kopp, C.; Hsiao, B. S.; Chu B. *J. Polym. Sci. Part B: Polym. Phys.* **2009,** *47*, 2288–2300.

28 Lala, N. L.; Ramaseshan, R.; Li, B. J.; Sundarrajan, S.; Barhate, R. S.; Liu, Y. J.; Ramakrishna S. *Biotechnol. Bioeng.* **2007,** *97*, 1357–1365.

29 Jalili, R.; Morshed, M.; Abdolkarim, S.; Ravandi H. *J. Appl. Polym. Sci.* **2006,** *101*, 4350–4357.

30 Gu, S. Y.; Ren, J.; Vancso, G. J. *Eur. Polym. J.* **2005,** *41*, 2559–2568.

31 Yuan, X. Y.; Zhang, Y. Y.; Dong, C. H.; Sheng J. *Polym. Int.* **2004,** *53*, 1704–1710.

32 Chang, K. H.; Lin, H. L. *J. Polym. Res.* **2009,** *16*, 611–622.

33 Tan, L. J.; Pan, D.; Pan N. *J. Appl. Polym. Sci.* **2008,** *110*, 3439–3447.

34 Lau, W. W. Y.; Guiver, M. D.; Matsuura T. *J. Memb. Sci.* **1991,** *59*, 219–227.

35 Arinstein, A.; Avrahami, R.; Zussman E. *J. Phys. D-Appl. Phys.* **2009, 42.**

36 McCann, J. T.; Marquez, M.; Xia, Y. N. *J. Am. Chem. Soc.* **2006,** *128*, 1436–1437.

37 Gupta, A.; Saquing, C. D.; Afshari, M.; Tonelli, A. E.; Khan, S. A.; Kotek R. *Macromolecules* **2009,** *42*, 709–715.